# LASER MONITORING OF AEROSOL POLLUTION OF AIR BASIN OF INDUSTRIAL CENTERS

**Yu.S. Balin and I.A. Rasenkov**

*Institute of Atmospheric Optics,*
*Siberian Branch of the Russian Academy of Sciences, Tomsk*
*Received December 9, 1992*

*A scanning single–frequency aerosol lidar is described in which a system of control, recording, and processing of information is based on a personal computer. The problem of processing of the lidar returns with instrumental noise is considered. The examples of lidar application to monitoring of the spatiotemporal distribution of aerosol polluting fields as well as determining the strength of emissions from stacks of local pollution sources are considered.*

## INTRODUCTION

Recently the pollution of the atmosphere of large industrial centers has been increased and in many cases it has already reached critical values.

As is well known, the basic elements of the available automated stations used for monitoring of the air basins of towns are ground–based stationary or mobile stations which cannot provide reliable spatial and temporal resolution.

At the same time to undertake some specific measures of salvaging our environment, one needs most comprehensive information about spatiotemporal distribution of pollutants over the air basin obtained in real time at altitudes up to at least 0.5–1 km and about the amount of harmful substances emitted by local sources into the atmosphere in a unit time.

Moreover, in many instances the increased concentration of pollutants in the atmosphere is determined by a meteorological potential and primarily by vertical temperature and wind stratifications in the atmosphere which must be monitored in real time as well.

Systems of remote sounding of the atmosphere, i.e., lidars, meet these requirements in full measure. The first lidar applications to monitoring of the spread of pollutants were reported in 1972 in Ref. 1. Then they were generalized in Ref. 2. In the domestic literature the problem of lidar application to the diagnostics of aerosol pollution was elucidated at length in Ref. 3.

Our paper deals with recent advances in developing the systems of remote ecological monitoring at the Institute of Atmospheric Optics.

## SYSTEMS OF REMOTE MONITORING OF AEROSOL POLLUTION

In a series of aerosol lidars developed at the Institute of Atmospheric Optics there are lidars of the LOZA type whose permanent modernization allows us to follow the principal trends in the development of such systems.

The LOZA–3 lidar is the base one in this series.[3] Since recently the general design of the lidar undergoes no substantial changes, here we omit the description of its construction in detail. It can be found elsewhere.[3]

The lidar equipment is installed in a cabin of an autovan with a microclimate system for the lidar to function properly in both summer and winter. A transceiver is an integrated unit positioned on an electromechanical scanning rotating column. From above the transceiver is covered with a metal dome protecting from unfavorable atmospheric conditions. When scanning in the azimuthal directions is performed, the dome rotates on a plummer bearing sinchronously with the transceiver. An emitting head of a laser and a TV camera for scanning of the space under study are positioned symmetrically on both sides of a receiving telescope. Power supply and cooling units are positioned at the base of the scanning rotating column.

The aerosol lidar complex belongs to a class of scanning–searching measuring systems and therefore it must suit to a set of performance specifications. The basic specifications are listed in Table I. The essential feature required of the lidar as a means for mapping of spatial distribution of pollutants in real time and estimating the strength of emissions from local sources is the provision of adequate spatial resolution. The lidar spatial resolution is determined by the range and angular resolution of the instrument. It is evident that the first component is determined by specifications of the transceiving unit and frequency response of the lidar measuring channel. The angular resolution is a function of the transmitter beam divergence and is determined by accuracy of control of the lidar scanning column.

The lidar under consideration was modernized compared to that previously used in Ref. 3 to improve exactly these specifications. This concerns first of all the lidar recording and control system which was developed based on an IBM PC/AT.

A device of digital recording of lidar returns was set in the standard of this computer and was built directly in a processor. A controller was based on an K1107 PV2 eight–bit analog–to–digital converter. It performed the following functions: synchronous digitizing of a lidar return, storage of digital information, arbitrary sample from lidar return with its subsequent output in a computer channel, program–controlled adjustment of zero bias of the analog–to–digital converter, and control with actuators of elevation angles of the lidar scanning column.

0235-6880/93/02 104-08 $02.00 

*TABLE I. Basic design specification of the LOZA–3 lidar.*

| Parameter | Dimension | Numerical value |
|---|---|---|
| Range and direction of sounding: | | |
| –Range of sounding of smoke plumes | Km | 5–7 |
| –Elevation angle | | |
| –Azimuth | deg | 10–90 |
| –Spatial resolution | deg | 0–340 |
| –Angular resolution | m | 7.5 |
| | min of arc | 10 |
| Transceiver: | | |
| Transmitter: | | LTI–405 |
| –Wavelength | | |
| –Energy per pulse | μm | 0.532 |
| –Pulse repetition frequency | mJ | 25 |
| –Pulse duration | Hz | 20 |
| –Collimator aperture | ns | 15 |
| | mm | 100 |
| Receiver: | | |
| –Receiving objective aperture | | |
| –Bandwidth of the interference filter | mm | 300 |
| | nm | 3 |
| Photodetector: | | |
| Television view finder | | |
| | | FEU–84 |
| Control and recording system: | | KTP–63 |
| –Computer | | |
| | | IBM |
| Analog–to–digital converter (ADC): | | PC/AT |
| –Word capacity | bit | |
| –Clock rate | MHz | |
| –Maximum amplitude of input signals | V | 8 |
| –Random–access memory capacity | kbite | 20 |
| | | 1 |
| | | 1(1024 readings in the sensing range) |
| | °C | from –20 |
| Operating conditions: | | to –40 |
| –Temperature | % | 95 |
| | hPa | 800–1000 |
| –Relative humidity | | 24 hours a day |
| –Pressure | | 6500/1000 |
| –Operating mode | kg | 220/380 V, 50 Hz, 5 kW |
| | – | |
| Mass of lidar/instruments | | |
| Power supply | | |

The VT–5 induction rotating transformers coupled through parasitic transmissions and installed at the output shafts of the turnable column are used as primary sensors. The sensors operate as phase invertors and provide an angle–phase–code transformation with an error less than 5′.

The rates of operation of all lidar units (pulse repetition rate, scanning rate of the turnable column sounding in the preset sectors of space, rate of lidar return digitizing and rate of data storage in the computer memory, and rate of digitizing, synchronization of the sensors of elevation angles) are rigidly bound and controlled by a resident microcomputer built in a control system based on a single–crystal computer.

The above–described lidar accomplishes two modes of operation. The first one is accomplished in the manual scanning regime in which displacement of a sounded object cannot be predicted and must be followed using a TV scanning system. Using the control system, an operator turns the column at the prescribed angular velocity within the preset sectors of horizontal and vertical scanning. In this case for each laser shot the information about the direction of sounding and the digitized values of lidar returns from the examined atmospheric objects are entered into the computer memory from the sensors of the elevation angles. The second type of operation is completely automated measurement controlled by a special program. It incorporates two basic regimes: position and sector scannings. In the position regime under instructions (Azimuth, Angle of elevation, and Angular velocity) keyed in by the operator, the optical axis of the lidar transceiver is set on the given point and is hold in this position during sounding. This regime is frequently used in sounding of plumes from local pollution sources to measure the strength of their emissions.

The information about the location of all stacks in the field of view of the lidar can be entered into the computer memory. This provides an alternate sounding of smoke plumes from each source with maximum possible spatiotemporal resolution.

In the case of sector scanning the trajectory of the lidar optical axis, i.e., scanning pattern, is also keyed in by the operator and has the following instruction format: Azimuth A1, Angle of elevation M1, Azimuth A2, Angle of elevation M2, Step, and Scanning velocity. Here (A1, M1) and (A2, M2) are the coordinates of the initial and end points of the sector in the space under study, Step is angular resolution between neighboring directions of sounding (in practice it is no less than 1°).

This regime is used for studying the general pattern of pollution distribution over the air basin of the town when mapping is carried out by obtaining several azimuthal sections at different angles of elevation. The angles are determined by the required angular resolution between the adjacent azimuthal sections as well as by maximum elevation height of aerosol pollution in the specific situation. Our experiments revealed that 5–10 sections are sufficient to obtain a complete pattern of aerosol pollution distribution in the industrial center.

In the regime of sector scanning the lidar is capable of sounding the atmosphere in several vertical planes at different azimuthal angles. The objective of such measurements is to determine the vertical distribution of aerosol pollution with the improved spatial resolution up to maximum altitudes in the regions with increased concentration of pollutants.

Each sounding step is organized into an individual data file. A serial number is assigned to this file which comprises a shot data sheet with measurement time and other specifications.

During the experiments in syncronism with the lidar measurements, the visual information was recorded on a video with the TV–camera. Thus some supplementary data were obtained for subsequent interpretation of the results of sounding.

The personal computer used in the system provided complete automation of measurements (including the control of lidar operation, computation of the measurable atmospheric parameters directly in the course of measurements), visualization, and archivation of the obtained information.

## TECHNIQUE FOR MEASUREMENT OF THE OPTO–PHYSICAL PARAMETERS OF AEROSOL FIELDS AND EMISSION STRENGTH

The data of laser sounding of aerosol fields are interpreted based on the lidar sounding equation which

relates the received signal power to the optical parameters of the atmosphere

$$P(z) = AG(z)\, z^{-2}\, \beta(z)\, \exp\left\{-2\int_0^z a(z')\, dz'\right\}, \qquad (1)$$

where $P(z)$ is the received signal power caused by scattering of laser radiation in the lidar direction, $z$ is the distance to the scattering volume along the sounding path, $A$ is the instrumental constant of the lidar, $G(z)$ is the geometric function of the lidar determined by the directional patterns of the transceiver, $\alpha(z)$ is the total volume scattering coefficient, and $\beta(z)$ is the volume backscattering coefficient.

As can be seen from Eq. (1), the received lidar return involves at least two unknown parameters $\alpha(z)$ and $\beta(z)$. Therefore, to solve the equation for one of the parameters, e.g., $\alpha(z)$, it is necessary to complete the problem. There are different ways of completing the lidar equation and hence different methods of its solution depending on the amount and quality of the available *a priori* information about the atmosphere. It is beyond the scope of this paper to describe all possible methods of solving this equation, especially as sufficiently complete reviews devoted to this problem were given in Refs. 3–5.

In the practice of laser sounding the methods based on analytical solution of the lidar equation[3,4] are most widely used. The method of asymptotic signal and the method based on calibration of the signal from the end point of the path to the known extinction coefficient are most appropriate for solving the above–formulated problem. Though the efficiency of the last method was first demonstrated in the domestic literature,[6,7] it was named for Klett after his paper has been published.[8] The advantage of these methods is that there is no need for absolute calibration of the lidar.

Without dwelling on the methodological problems described at length in Ref. 3, we deal with the effect of instrumental noise in the Klett technique as well as with some methods of reducing their effect on the error in the reconstructed optical parameters.

The instrumental drawbacks of the lidar are manifested in recording of, the lidar returns with ADC's which possess a limited word capacity and, hence, limited accuracy of signal digitizing. In our case of the eight–bit ADC we have 256 increments of signal amplitude.

The specific feature of lidar returns according to Eq. (1) is their sharp decrease as the reciprocal square of the distance. Therefore, for the lidars with moderate range of action (e.g., LOZA–3) the amplitude of the lidar return at distances longer than 2–3 km can be no more than 5–10 readings of the ADC even from local sufficiently thick aerosol formations. The methods of lidar data inversion, as a rule, make use of not the signal $P(z)$ but some $S$–function being equal to $S(z) = P(z)\, z^2$. The random noise in combination with limited accuracy of data recording results in substantial distortions of the $S$–function and, consequently, in large errors in reconstructing $\alpha(z)$ which at the end of the path can be several hundreds of percent.

The above–discussed points are illustrated by Figs. 1 and 2. The results of field measurements of aerosol polluting fields using the LOZA–3 lidar are shown in Fig. 1.

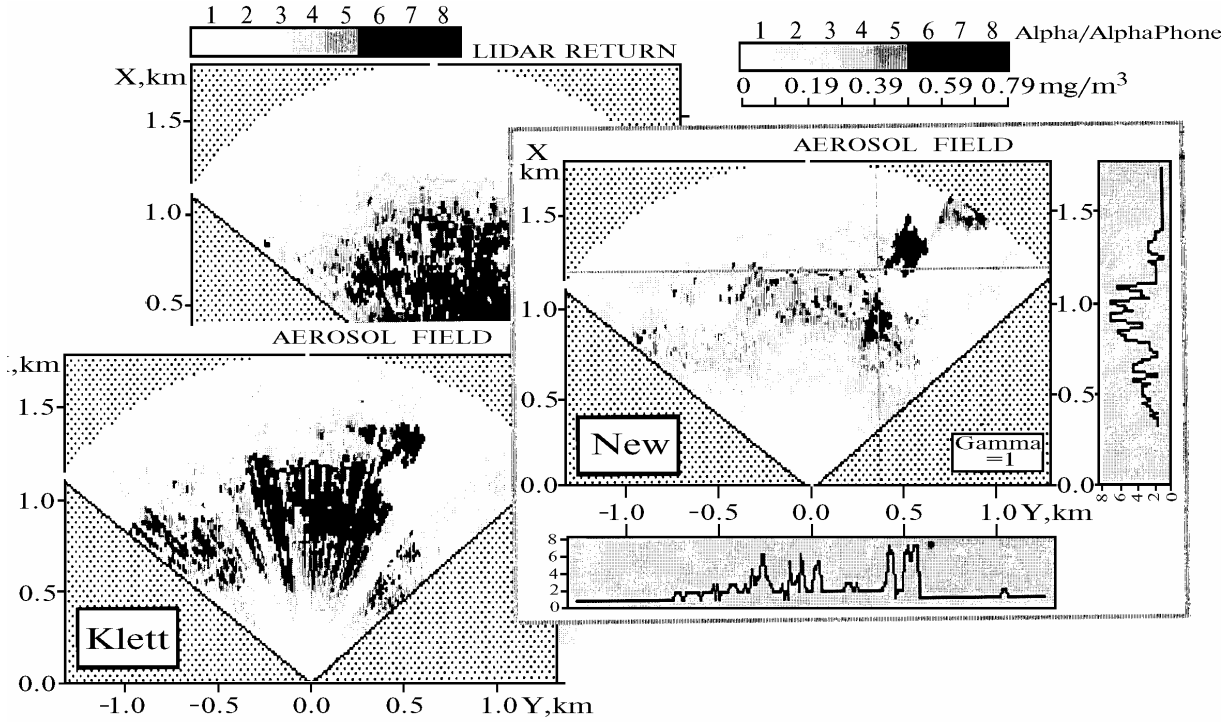


*FIG. 1. Comparison of the results of reconstruction of the opto–physical parameters of aerosol fields from experimental data by different methods.*

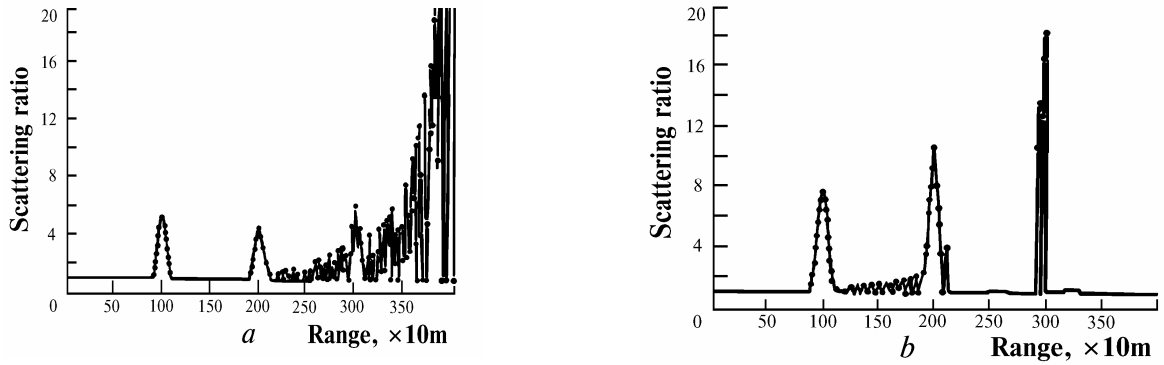


*FIG. 2. Comparison of the results of model calculation in reconstructing the scattering coefficient profiles by different methods: a) Klett method, noise $\Delta N = 4$ and b) iterative method, noise $\Delta N = 4$, and threshold $\Delta P = 5$.*

Displayed at the top of Fig. 1 is the field of lidar returns $P(z)$ while at the bottom of this figure the results of reconstruction by the Klett technique are illustrated. The point 0 indicates the lidar location. As can be seen from the figure, nonphysical pattern of an aerosol field in the form of alternating black and white bands of aerosol concentration has been obtained.

The same conclusion can be drawn from Fig. 2*a* illustrating the results of numerical modeling. The model profile of the scattering coefficient was taken in the form of a uniform background profile ($\alpha(z) = 0.2$ km$^{-1}$) on which three peaks corresponding to aerosol formations 200 m wide were superimposed at distances of 1, 2, and 3 km. The maximum value of the scattering coefficients for these formations was eight times larger. In the figure the ratio of the coefficients is plotted on the ordinate.

The signals $F(z)$ and $S(z)$ were calculated from Eq. (1) with white noise. The signal $F(z)$ was normalized so that its maximum was equal to the maximum code of the ADC, i.e., using an entire dynamic range of the converter. The noise was simulated on a computer with a random–number generator and the noise extreme value $\Delta N = 4$. Figure 2*a* clearly illustrates the deviation of the reconstructed values of $\alpha(z)$ from the model ones (by about a factor of two) for the first half the path and complete loss of information on the end sections of the path.

These disadvantages can be eliminated by modifying the method in the following manner.

Some value of the signal threshold $\Delta P$ is introduced, it is equal to or larger than the ADC code corresponding to a noise track (signal at long distances from the lidar). Then the signal below the threshold level $\Delta P$ is not recorded and the $S$–function corresponding to these distances is extrapolated

$$S^m(z) = \begin{cases} \dfrac{P(z)\, z^2}{G(z)}, & \text{for } P(z) \geq \Delta P \\ \dfrac{DP\, z^2}{G(z)} \exp\left\{ -2 \displaystyle\int_{z_{\text{th}}}^{z} \alpha^{m-1}(z')\, \mathrm{d}\, z' \right\}, & \text{for } P(z) < \Delta P, \end{cases} \qquad (2)$$

where $m = 1, 2, 3, \ldots$ .

Here the superscript $m$ is the iteration number and $z_{th}$ is the distance starting from which the signal amplitude becomes less than the threshold $\Delta P$.

In the case of sounding of smoke plumes the signal can repeatedly exceed the noise level, but it does not limit the application of the suggested procedure of data processing. The quantity $\alpha^0(z)$ being equal to its background value can be taken as the first iteration while the iterative algorithm is described by the following relation:

$$\alpha^m(z) = \frac{S^m(z)}{\dfrac{S_e^m}{\alpha_e} + \displaystyle\int_z^{z_e} S^m(z')\, \mathrm{d}z'}, \qquad (3)$$

where $S_e$ and $\alpha_e$ are the $S$–function and the scattering coefficient at the end of the path. The quantity $\alpha_e$ is usually assumed to be equal to its background value.

Relation (3) is reduced to the Klett technique in its conventional form for $\Delta P = 0$ and $m = 1$.

The results of implementation of this technique to processing of the same model signals are depicted in Fig. 2*b*. Since the noise code $\Delta N = 4$, the threshold $\Delta P$ was chosen to be equal to five. The calculations were interrupted at the fifth iteration for which the calculated integrals of the scattering coefficients along the path differed by less than 1%. It can be seen from the plots that the errors in reconstructing the scattering coefficients decrease substantially. We also modelled a situation with the threshold $\Delta P$ being sufficiently high, in which we lost the signal from the third aerosol formation located at the end of the path. Nevertheless, this fact did not affect the errors in reconstructing $\alpha(z)$ on the preceding sections of the path.

The efficiency of the above–described procedure for signal processing was supported by the field measurements. This clearly shows a pattern of the aerosol section represented at the right of Fig. 1.

The next important step in the problem of interpreting the sounding data is to estimate the aerosol mass concentration based on the information about its optical parameters. In general, the relation of the extinction coefficient to the concentration is a complicated function of particle composition, shapes, and size distribution. In Ref. 3 the proportionality coefficient $\mu$ between these characteristics was investigated both theoretically and experimentally. It was demonstrated that under real conditions the large variations $\mu = (0.52 \pm 0.34)$ mg·km/m$^3$ should be expected. The main role here is played by aerosol distinguishing features which are influenced by its microoptical and microphysical characteristics.[2] Nevertheless, in the review presented in

Ref. 9 a high correlation between optical thickness and mass concentration of aerosol for each individual emission source was reported based on the analysis of studies of different industrial plumes. Moreover, for some types of smokes the coefficient $\mu$ remained practically unchanged under different meteorological conditions. This is typical of the smokes in which the mean radius of aerosol particles corresponds to the Mie parameter $1 < \rho < 3$–$6$ as well as of the smokes which contain weakly hygroscopic particles.

For this reason to reduce the error in estimating the mass concentration from optical measurements, each specific region requires preliminary empirical studies or at least classification of aerosol type depending on the type of the polluting source.

To this point we have discussed mapping of aerosol pollutions based on the level of their maximum permissible concentration (MPC, mg/m$^3$). The other important parameter used in ecological monitoring is the strength of pollution emission, i.e., the amount of harmful matter emitted into the atmosphere in a unit time (g/s).

Different methods can be employed to evaluate the strength of emission using the lidar. One of them is the azimuthal scanning in the ground layer of the atmosphere along the paths perpendicular to the direction of plume spreading. By determining the extremum of optical thickness on these paths it is possible to estimate the emission strength based on the relations derived in Ref. 10. In this case the information about the wind velocity field, coefficients of turbulent diffusion, and rate of sedimentation of the particles with different size is needed. It is clear that practical implementation of the proposed technique is difficult. The reasons are a large number of additionally measurable parameters and the fact that the optical state of the ground layer of the atmosphere is affected by many other sources of pollution.

The other method is direct sounding of an entire section of the plume either in vertical or horizontal plane. Below, for definiteness, we consider scanning in the vertical plane.

Based on simple assumptions, it is not difficult to derive the relation for the emission strength $B$(g/s)

$$B = V \mu \cos\varphi \int_S \alpha(S')\, dS' , \qquad (4)$$

where $V$ is the velocity of aerosol transport in the plume, $S$ is the section of the plume in the vertical plane, $\alpha(S')$ is a two–dimensional function describing the scattering coefficient distribution over the plane $S'$.

The angle $\varphi$ takes into account the fact that the direction of sounding was not perpendicular to that of spreading of the smoke plume.

The feasibility of determining the parameters $\mu$ and $\alpha(S')$ was discussed previously. It should be noted, however, that to reduce the error in determining the integral in Eq. (4), the vertical scanning of the smoke plume must be carried out with maximum spatio–angular resolution available for this class of instruments.

The angle $\varphi$ is determined with a sufficient accuracy from the analysis of horizontal sections of the plume, since all sounding directions can be related to the absolute angular system of coordinates.

There are several methods of measuring the rate of aerosol transport. The traditional one is the use of the Dickon exponential law[11] for the first several hundreds of meters of the ground layer of the atmosphere. Following this law it is possible to approximate the wind profile up to the preset altitudes by measuring its velocity at a standard altitude, for example, with a conventional local sensor. The exponent varies from unity to zero and depends on the class of atmospheric stability and the type of the underlying surface. It is clear that the direct measurements of wind velocity, which can be carried out with the same lidar, are preferred.

The physical foundation for lidar measurements of transport velocity is the wind entrainment of aerosol particles in the plume. Smoke plume spreading and evolution engenders a random field of inhomogeneities of aerosol particle concentration. For this reason a set of spatiotemporal samples recorded by the lidar is also of a random character. The methods of correlation and spectral analysis are widely used[12] to extract the characteristics of wind velocity for statistical description of the obtained data file.

The velocity is measured by step–by–step sounding of the plume and storing the statistical information about the signal amplitudes recorded at least from two ranges. The distance between them is the base of measurements. If the correlation analysis is used, the temporal cross–correlation function is calculated. By taking the ratio of the base to the time delay between maxima of these functions, it is possible to determine the absolute value of wind velocity.

In the spectral analysis the cross–spectra and then the phase function are calculated. The latter depends on time of spreading of aerosol inhomogeneity between the measurable points of the path. It is determined by the base and observed wind velocity. That provides the basis for the estimation of the wind velocity. In both cases the radial component of wind velocity is measured. However, by knowing relative directions of sounding and plume spreading, it is possible to calculate the value of transport velocity.

In conclusion of this section we would like to dwell on one more problem which is connected with the choice of location of lidar section of a smoke plume. This choice must not be random since it depends on both engineering possibilities of the lidar and some other methodological peculiarities.

The majority of production processes lead, as a rule, to the emission of not only solid aerosol particles but also of a large amount of water vapor into the atmosphere. In Ref. 13 it was pointed out that this can lead to the formation of regions of local supersaturation and, consequently, to sharp growth of water coating of aerosol particles.

As follows from theoretical calculations,[13] the behavior of relative humidity along the axis of smoke plume is of extremal character attaining its minimum near the mouth of the stack and its maximum at a distance of 300–400 m from it depending on meteorological conditions and the parameters of emission. The zone of moistened ash particles in this case is extended for about 1000 m.

Based on the calculational results, it is natural to conclude that sounding must be carried out either directly above the mouth of the stack or in the far zone of the plume. However, small geometric dimensions of plume over the mouth of the stack can be beyond the limits of angular and spatial resolution of the lidar. Moreover, high particle concentration at the site of emission results in a wide dynamic range of variation in a signal. This in its turn can lead to the loss of primary information under conditions of limited word capacity of the ADC.

Some problems arise in the case of sounding in the far zone. At such distances the plume is no longer an integrated formation and separates into several parts under the action of atmospheric turbulence. Moreover, in the case of sounding in the region with several polluting sources,

the probability of the event that at high altitudes all smoke plumes emerge into one aerosol field is high.

Summing up the above–discussed problems, it should be noted that there exists some optimal distance from the stack of the polluting source at which the entire smoke plume must be completely intercepted by a scanning section. The analysis of theoretical calculations and experimental results shows that this distance is about 50–100 m.

Such are some methodological and engineering aspects of the problem of laser sounding of aerosol pollution.

## RESULTS OF EXPERIMENTAL STUDIES

In this section we present the results of remote laser monitoring of air basins in Kemerovo and Pavlodar. In Kemerovo there are many large industrial enterprises ( SRPS, coking by–product plant, Production Union "Azot", etc.) which are located close to each other. In Pavlodar the industrial enterprises are located at large distances from each other. Therefore, we present here mainly the results obtained in Kemerovo.

The measurements were carried out from October 24 to November 2, 1990. Land forms allowed us to install the lidar on the right elevated bank of the river Tom'. The buildings of industrial enterprises were on the other flat bank.

A schematic map of the region under study is shown in Fig. 3 where squares stand for stacks of the largest sources of pollution.

Four–six cycles of measurements were usually carried out per day, each included five horizontal sections in the azimuthal sector enclosed between the angles of 0 and 115° and four vertical sections in the sector enclosed between the elevation angles of 0 and 24°. The azimuthal scanning angles were 0, 2.5, 5, 7.5, and 10° with respect to the horizon. Angular resolution between the sounding directions was 1° and spatial resolution along the path was 15 m. The maximum sensing range was 4.5 km. Thus, in each horizontal section there were 116 signals with 300 counts per signal. The vertical sections were obtained with 0.2° angular resolution which corresponded to 120 signals in one section.

Figures 3 and 4 illustrate the results of mapping of the distribution of opto–physical parameters (scattering coefficient and mass concentration) of aerosol polluting fields over the air basin of the town. At the top left of the figures the structure of a measurement file is listed which indicates the serial numbers of expeditions, measurement cycles, and sections. A type of section (horizontal or vertical) is denoted by letters at the end of the file.

Such a structure of the file enables one to archive the data easily for subsequent statistical processing of the stored data files.

The aerosol concentration distribution over the section is displayed by different degree of blackening, whose gradations are given at the bottom of the figures. This image graphics provides a semiquantitative pattern of aerosol field concentration distribution. At the same time, since it is constructed from a digital data array being in the computer memory, we always can extract the quantitative information for any point of the map. One of possible schemes of extracting the information using horizontal and vertical cursors has been already shown in Fig. 1.

The above–described sections were obtained successively at elevation angles of 7.5 and 10° that enabled one to estimate the difference between the spatial distributions of pollution at different altitudes. One of such differences is manifested in recording of smoke plume from the SRPS stack whose mouth is at an altitude of 150 m (Fig. 4, a square with coordinates $x = -0.6, -1.2$; $y = 0.6, 1.2$) at large angles.

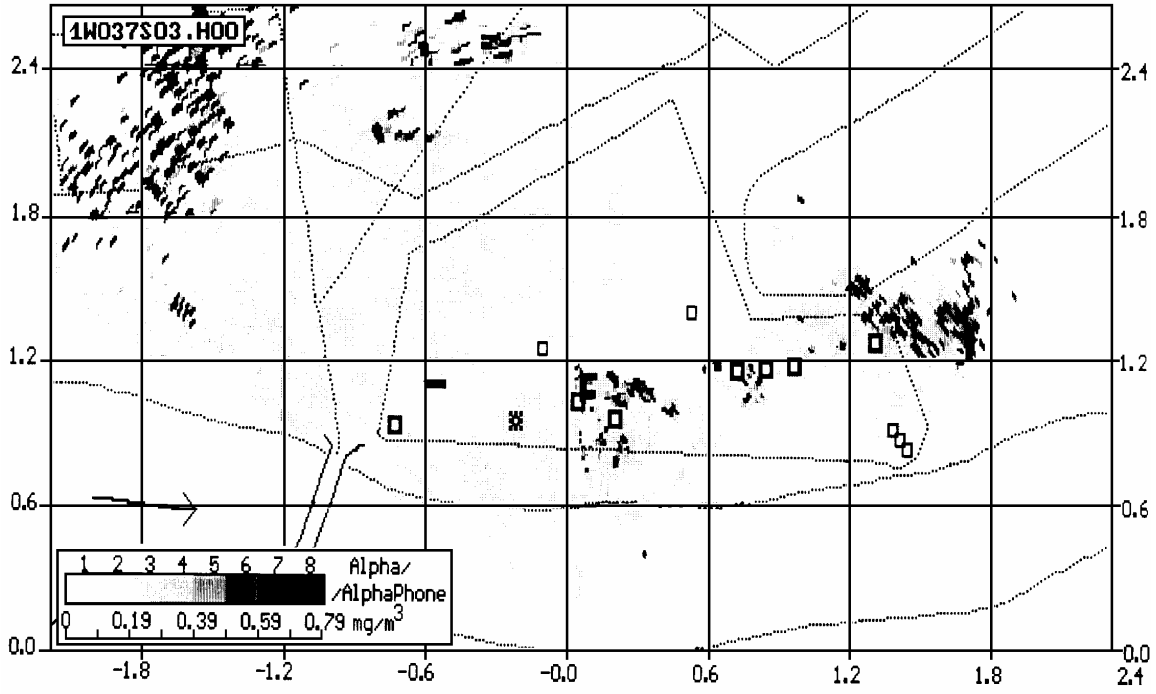


*FIG. 3. Mapping of aerosol pollution distribution in the case of azimuthal scanning at an elevation angle of* 7.5° *in Kemerovo. Point* 0 *denotes the lidar location.*

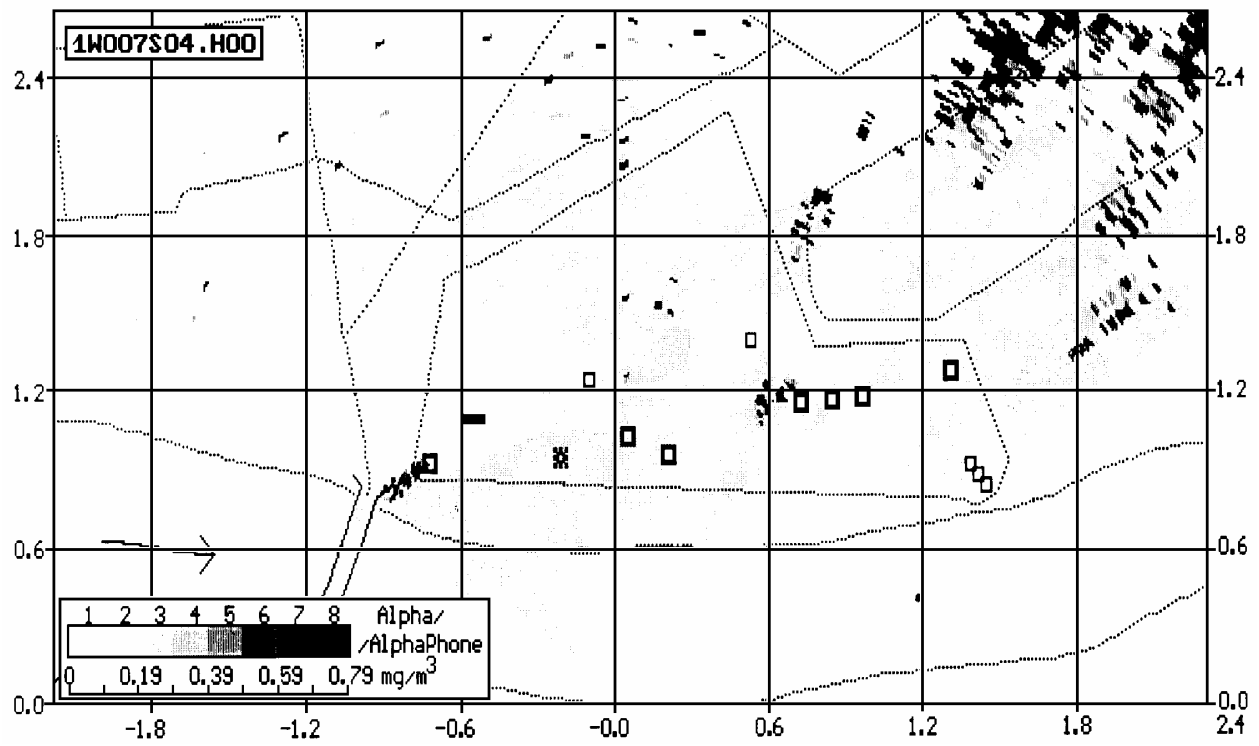


*FIG. 4. The same as in Fig. 3 but at an elevation angle of* 10°.

This source by its topographic characteristics (height of the stack, distance from the other sources) differs substantially from the other objects and its smoke plume is always distinquishable against the background field of pollution. That is why the SRPC emissions were the subject of specific studies which consisted in sounding of the atmosphere in the region of mouth of the stack with maximum spatio–angular resolution (sector 35 × 12°).

The time required for obtaining the azimuthal section of general view was 20 s, the atmospheric volume being monitored was 2.6 $km^3$.

Since the type of azimuthal sections obtained the other days is roughly similar to the above–described sections, it is expedient to present all results briefly. We calculated the total mass of aerosol substance and its concentration in the entire examined volume (13.2 $km^3$ for five azimuthal sections) and in the volume containing the plume from the SRPS (0.4 $km^{-3}$).

Selected results calculated for several days are tabulated in Table II. In the column "Section of general view" insignificant variations of the measurable parameters depending on the days of observations have engaged our attention. This can be due to the fact that in a large volume of the space being monitored all emissions from local sources are averaged, and during a short period of observations no substantial changes were observed both in meteorological situation and regimes of operation of many enterprises.

In the case of sounding of the atmosphere with a smaller volume of averaging, the variation of the parameters should grow large. This is evident from the other column of the table. It should be noted that variations were observed both in the course of one day and from day to day.

In the light of the above–discussed problems it is interesting to follow the temporal dynamics of the emission strength from one and the same SRPS stack. To this end, by vertical scanning with 0.2° resolution we obtained cross sections of the smoke plume at distances of 50, 100, and 150 m from the stack. These cross sections are displayed in Fig. 5. Each cycle contains 10 sections but only first five of them are displayed in the figure. The time interval between the sections of one cycle was 2 min.

As can be seen from the figure, the transverse size of the plume increases as the distances from the source become larger. In addition, in the far zone it keeps its integral structure (Figs. 5*b* and *c*). However, in the near zone the plume disintegrates into two parts equal in size. We think that the lower part of the plume is engendered by sedimentation of coarsely dispersed fraction of ash particles which comes into play in the immediate vicinity of the mouth of the stack. But this pattern was not observed in the subsequent cycles (Figs. 5*b* and *c*) which indicates the fact that the sedimentation zone is limited to 100 m.

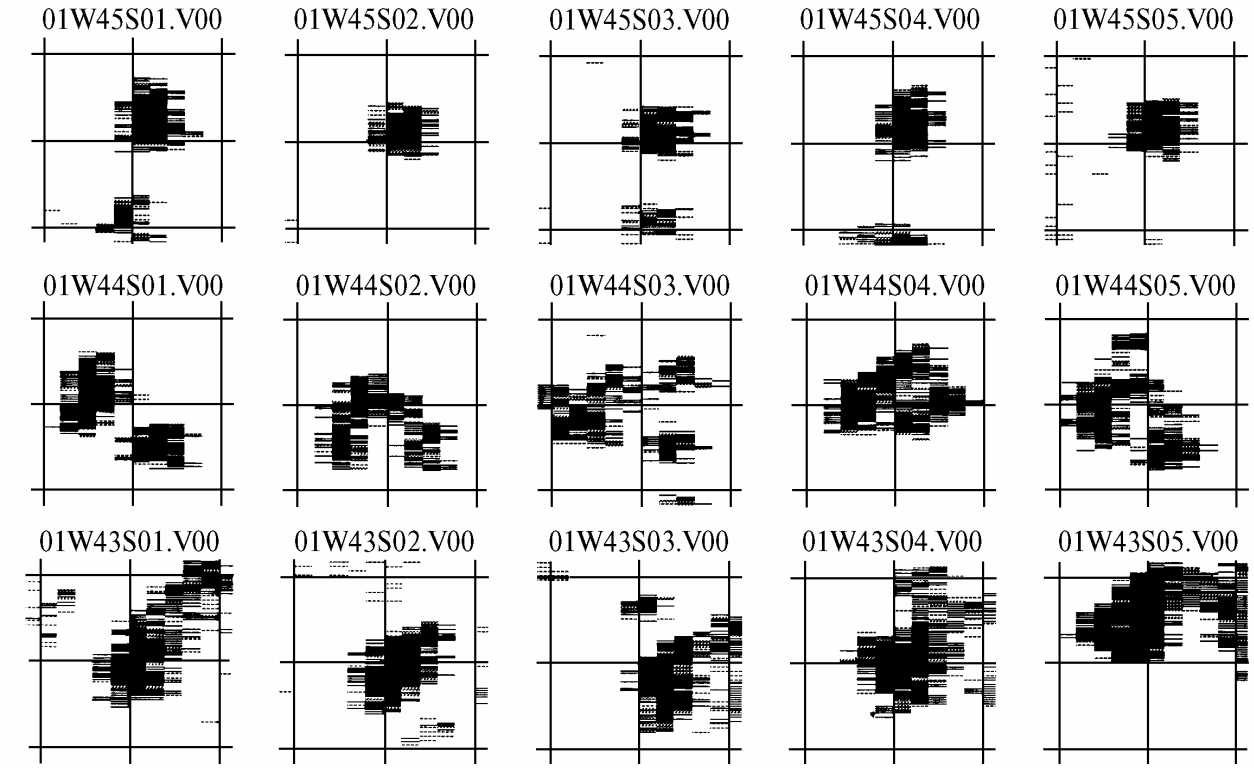


*FIG. 5. Vertical sections of the SRPS smoke plume vs time (2 min interval) and distance of* 50 *(upper row),* 100*, and* 150 *m from the mouth of the stack. The scaling grid square is* 75 × 75 *m.*

*TABLE II. Results of measurements of aerosol pollution.*

| Serial number of cycle | Date, time | Section of general view | | Section above the SRPS stack | |
|---|---|---|---|---|---|
| | | Mass, kg | Concentration, mg/m$^3$ | Mass, kg | Concentration, mg/m$^3$ |
| | October 25 | | | | |
| 4 | 9:00 | 1850 | 0.14 | 180 | 0.45 |
| 5 | 11:00 | 1600 | 0.12 | 150 | 0.38 |
| 6 | 14:00 | 1480 | 0.11 | 136 | 0.34 |
| 7 | 16:00 | 1750 | 0.13 | 170 | 0.42 |
| 8 | 18:00 | 1500 | 0.11 | 200 | 0.50 |
| | October 28 | | | | |
| 16 | 9:00 | 1470 | 0.11 | 350 | 0.88 |
| 17 | 12:00 | 1550 | 0.12 | 300 | 0.75 |
| 18 | 14:00 | 1420 | 0.11 | 280 | 0.70 |
| 19 | 18:00 | 1700 | 0.13 | 170 | 0.42 |
| 20 | 20:00 | 1650 | 0.12 | 250 | 0.62 |
| | October 29 | | | | |
| 21 | 9:00 | 1350 | 0.1 | 320 | 0.80 |
| 22 | 12:00 | 1500 | 0.11 | 250 | 0.62 |
| 23 | 14:00 | 1600 | 0.12 | 280 | 0.70 |
| 24 | 18:00 | 1560 | 0.12 | 140 | 0.35 |
| 25 | 20:00 | 1400 | 0.10 | 220 | 0.55 |
| | November 1 | | | | |
| 30 | 9:00 | 1400 | 0.10 | 220 | 0.55 |
| 31 | 12:00 | 1600 | 0.12 | 300 | 0.75 |
| 32 | 14:00 | 1570 | 0.12 | 400 | 1.00 |
| 33 | 19:00 | 1380 | 0.10 | 130 | 0.33 |
| 34 | 21:00 | 1400 | 0.10 | 200 | 0.50 |
| 35 | 23:00 | 1280 | 0.11 | 126 | 0.31 |

This supports once again the need for an estimate of the emission strength over the plume sections at distances closer to the pollution source.

To make this estimate, we first measured the velocity of plume spreading using the lidar. The experimental velocity of plume spreading was about 10 m/s.

Another possible way of determining the plume spreading velocity in the direction perpendicular to the line of sight is the use of the TV system which was developed for entering the TV signals into a personal computer. Then the correlation analysis of smoke plume images taken at definite intervals was made. The simultaneously taken dimensions of the mouth of the stack of the pollution source served as the spatial scale in this case.

The measurement results of the unknown component of plume spreading velocity were the same as in the lidar experiments. The vertical component was about 2 m/s.

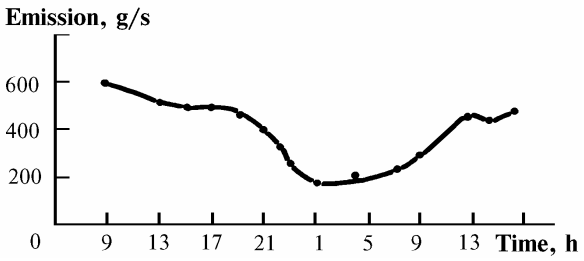


*FIG. 6. Temporal behavior of the strength of emission of the pollution from the SRPS stack obtained on November* 1–2, 1990.

The strength of emission from the SRPS stack was estimated from the obtained values of the spreading velocity and mass concentration in the plume section (50 m) for several hours. The temporal behavior of variations of this parameter is shown in Fig. 6. Depicted in the figure is the clearly pronounced dynamics of the emission strength which is far beyond the limits of possible measurement errors. It is clear that to estimate reliably these errors one must carry out a series of tests using, e.g., direct measurements in gas pipelines connecting the stack with boilers of the heat–and–power station.

However, in these studies we failed to make such comparison due to the lack of the required instrument and attending personal which could simultaneously monitor more than ten of gas pipelines.

At a later time simultaneous operation of one more remote means at the mouth of the stack can be considered as one of the possible ways of joint calibration. This is a Raman scattering lidar based on recording the spectra of Raman scattering radiation.[14]

For the same purpose the lidar was used in monitoring of the air basin of Pavlodar located in a plain with large enterprises being widely spaced. The plants of the town Ermak situated at a 15–km distance from Pavlodar bring a definite amount of pollutants into the atmosphere of this city. Taking into account the above–described situation, the problem was formulated as follows. The lidar must be installed on the roof of the highest building of the town and must provide the monitoring range of the atmosphere up to 7–10 km.

An LTI–407 laser with 80 mJ energy per pulse was used to increase the lidar potential. The rest of the lidar parameters corresponded to the specifications listed in Table I.

The lidar transceiver was installed under a protective rotating dome on the roof of a 12–storied building and the control and recording instrument was positioned in the room of the upper floor.

The azimuthal section displayed below illustrates one more possible data format (Fig. 7). A map of aerosol pollutant distribution is given in a rectangular system of coordinates with 1 × 1 km scaling grid . The aerosol field was recorded with 1° angular and 60–m spatial resolutions. The magnitude of mass concentration is given directly in each square of the map being a value averaged over this area.

The empty fragment of the figure is that region of the town without sources of pollution which was not studied. The lidar was located at the point of intersection of south and east boundaries of this zone.

The separated central part of the figure illustrates the feasibilities of lidar monitoring of spreading of the smoke plumes at large distances. In this case high–power sources of pollution of the aluminium and tractor plants were remotely monitored.

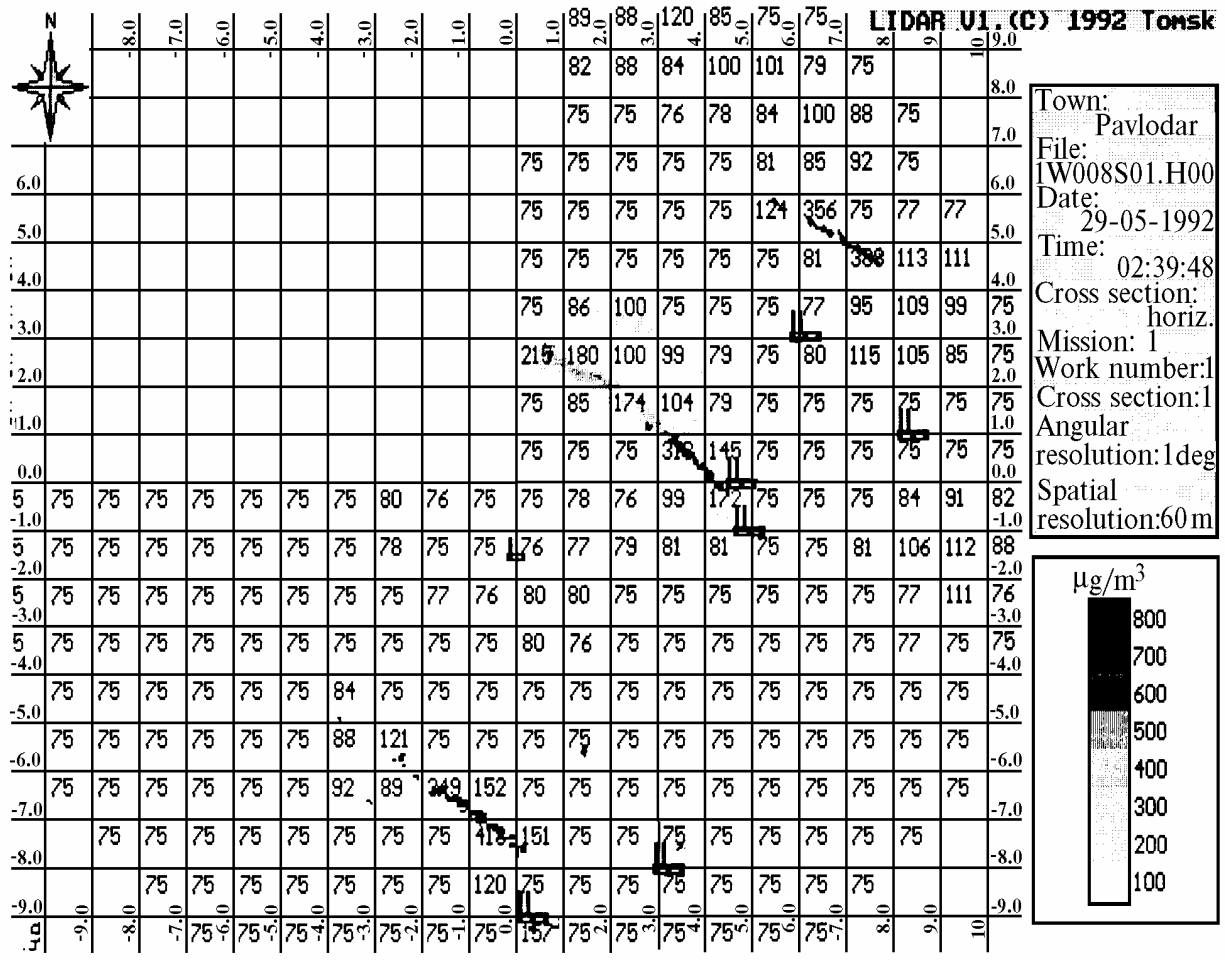


*FIG. 7. Mapping of aerosol pollution distribution in the case of azimuthal scanning at an elevation angle of 2° in Pavlodar.*

Any fragment of the map whose dimensions can be smaller than that of the scaling grid or equal to that of the combination of squares can be displayed at magnification, if required. As an illustration, Fig. 8 displays a fragment of the central part of Fig. 7 in more detail.

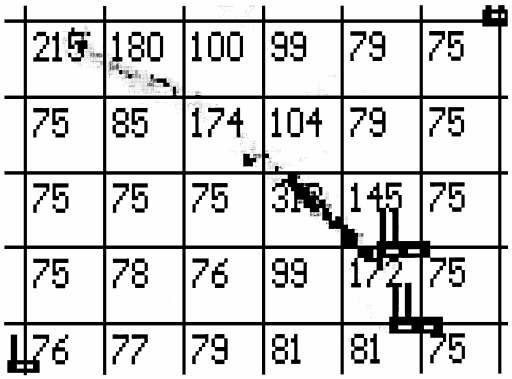


*FIG. 8. Magnified fragment of the image of the central part of Fig. 7.*

It is apparent that some specific modes of lidar operation including data format can be required for every town. The available level of engineering and software enables one to adapt easily the modes of lidar operation to any specific conditions.

## CONCLUSION

The information presented in this paper describes the lidar potentialities and the problems which arise in lidar application to ecological monitoring of the urban air basin.

Further prospects of lidar reduction to practice should be associated with the use of specialized optimal noise–proof algorithms of lidar return processing based, e.g., on a statistical approach[15] and further improvement of the sounding technique.

That is why a specialized portable scanning lidar which can be installed on the roofs of buildings and on movable carriers is being developed at present at the Institute of Atmospheric Optics.

In addition, one of the most important stages of its reduction to practice is ecological and metrological certification of lidars.

The authors thank their colleagues from the Institute of Atmospheric Optics G.S. Bairashin, A.P. Rostov, and A.M. Sutormin for large contribution to the development of the lidar used in the measurements.

## REFERENCES

1. R.T.H. Collis and E.E. Uthe, Opto–Electron. **4**, No. 2, 87 (1972).
2. E.D. Hinkley, ed., *Laser Monitoring of the Atmosphere* [Springler Verlag, New York, 1976).
3. M.V. Kabanov, ed., *Laser Sounding of Industrial Aerosols* (Nauka, Novosibirsk, 1986), 186 pp.
4. V.E. Zuev, ed., *Signals and Noise in Laser Sounding* (Radio i Svyaz', Moscow, 1985), 264 pp.
5. V.E. Zuev, G.M. Krekov, and M.M. Krekova, in: *Remote Sounding of the Atmosphere* (Nauka, Novosibirsk, 1978), pp 3–40.
6. S.I. Kavkyanov, in: *Abstracts of Reports at the Fourth All–Union Symposium on Laser Sounding of the Atmosphere,* Tomsk (1976), pp. 95–98.
7. V.E. Zuev, G.O. Zadde, S.I. Kavkyanov, and B.V. Kaul', in: *Remote Sounding of the Atmosphere* (Nauka, Novosibirsk, 1978), pp. 60–68.
8. J.D. Klett, Appl. Opt. **20**, 211 (1981).
9. D.B. Uvarov and G.P. Zhukov, in: *Proceedings of the Institute of Experimental Meteorology*, No. 15(60) (1976), pp. 100–117.
10. A.A. Antonovich, G.O. Zadde, and A.V. Podanev, Atm. Opt. **3**, No. 9, 873–876 (1990).
11. K. York and S. Yorner, *Air Pollution* [Russian translation] (Mir, Moscow, 1980), 539 pp.
12. I.V. Samokhvalov, ed., *Correlation Methods of Laser Radar Measurements of Wind Velocity* (Nauka, Novosibirsk, 1985), 222 pp.
13. Yu.E. Geints and A.A. Zemlyanov, Atm. Oceanic Opt. **5**, No. 5, 337–342 (1992).
14. Yu.F. Arshinov, S.M. Bobrovnikov, V.K. Shumskii, et al., Atm. Oceanic Opt. **5**, No. 5, 323–328 (1992).
15. G.M. Krekov, S.I. Kavkyanov, and M.M. Krekova, *Interpretation in Signals of Laser Sounding of the Atmosphere* (Nauka, Novosibirsk, 1987), 240 pp.